EXCIMER LASER RESEARCH

C. A. Brau, et al

Avco Everett Research Laboratory,
Incorporated

Prepared for:

Office of Naval Research
Advanced Research Projects Agency

August 1975

EXCIMER LASER RESEARCH

SEMI-ANNUAL TECHNICAL REPORT

for the period

August 15, 1974 to February 15, 1975

Contract No. N00014-75-C-0063

August 1975

sponsored by

ADVANCED RESEARCH PROJECTS AGENCY

ARPA Order No. 1806

AVCO EVERETT RESEARCH LABORATORY, INC.

A SUBSIDIARY OF AVCO CORPORATION

53

UNCLASSIFIED

SECURITY CLASSIFICATION OF THIS PAGE (When Date Entered)

REPORT DOCUMENTATION PAGE		READ INSTRUCTIONS BEFORE COMPLETING FORM
1. REPORT NUMBER	2. GOVT ACCESSION NO.	3. RECIPIENT'S CATALOG NUMBER
4. TITLE (and Subtitle) EXCIMER LASER RESEARCH		5. TYPE OF REPORT & PERIOD COVERED Semi-Annual Technical Rpt. Aug. 15, 1974-Feb. 15, 1975 6. PERFORMING ORG. REPORT NUMBER N00014-75-C-0063
7. AUTHOR(s) C. A. Brau and J. J. Ewing		8. CONTRACT OR GRANT NUMBER(s)
9. PERFORMING ORGANIZATION NAME AND ADDRESS Avco Everett Research Laboratory, Inc., 2385 Revere Beach Parkway Everett, Massachusetts 02149		10. PROGRAM ELEMENT, PROJECT, TASK AREA & WORK UNIT NUMBERS Program Code No. 5E20
11. CONTROLLING OFFICE NAME AND ADDRESS Advanced Research Projects Agency ARPA Order No. 1806		12. REPORT DATE August 1975 13. NUMBER OF PAGES 47
14. MONITORING AGENCY NAME & ADDRESS(if different from Controlling Office) Office of Naval Research Department of the Navy 800 North Quincy Street Arlington, Virginia 22217		15. SECURITY CLASS. (of this report) Unclassified 15a. DECLASSIFICATION/DOWNGRADING SCHEDULE

16. DISTRIBUTION STATEMENT (of this Report)

DISTRIBUTION STATEMENT A
Approved for public release;
Distribution Unlimited

17. DISTRIBUTION STATEMENT (of the abstract entered in Block 20, if different from Report)

18. SUPPLEMENTARY NOTES

19. KEY WORDS (Continue on reverse side if necessary and identify by block number)

1. Excimer
2. Lasers
3. Electron Beams
4. Rare Gas Halides

20. ABSTRACT (Continue on reverse side if necessary and identify by block number)

This report describes a theoretical and experimental investigation of the rare gas monohalides. As a class, these molecules show great promise for achieving high power acalable laser action in the near UV portion of the spectrum.

A theory has been developed to describe the structure of these molecules. The predictions of this theory are borne out by fluorescence experiments

DD FORM 1 JAN 73 1473 EDITION OF 1 NOV 65 IS OBSOLETE

UNCLASSIFIED

SECURITY CLASSIFICATION OF THIS PAGE (When Date Entered)

(20)
carried out in high pressure rare gas/halogen mixtures, using electron-beam excitation.

The kinetics of these mixtures and their potential as high power lasers are discussed.

FOREWORD

ARPA Order No: 1806

Program Code No: 5E20

Name of Contractor: Avco Everett Research Laboratory, Inc.

Contract Expiration Date: August 14, 1975

Amount of Contract: $171,295

Contract No: N00014-75-C-0063

Principal Investigator and Phone No: C. A. Brau
617-389-3000 Ext. 532

Scientific Officer: Director, Physics Program, Physical Sciences Division
Office of Naval Research, Department of the Navy
800 North Quincy Street
Arlington, Virginia 22217

Short Title of Work: Excimer Laser Research

ABSTRACT

This report describes a theoretical and experimental investigation of the rare gas monohalides. As a class, these molecules show great promise for achieving high power scalable laser action in the near UV portion of the spectrum.

A theory has been developed to describe the structure of these molecules. The predictions of this theory are borne out by fluorescence experiments carried out in high pressure rare gas/halogen mixtures, using electron-beam excitation.

The kinetics of these mixtures and their potential as high power lasers are discussed.

TABLE OF CONTENTS

LIST OF ILLUSTRATIONS

I. INTRODUCTION

The primary objective of the present ARPA high-energy laser program is to identify lasers which are capable of being used at high power levels and long ranges. The long ranges tend to favor shorter wavelength lasers since they can be focused more sharply. However, large aperture infrared chemical lasers appear to be possible and, in fact, establish the minimum performance requirements for any new laser which may be developed. Of course, the minimum performance requirements will depend upon the wavelength and other considerations. However, it appears that for an electrical laser operating in the visible or near ultraviolet portion of the spectrum to be competitive with a chemical system, it must offer an efficiency greater than about 15 to 20% and be able to operate at power levels in excess of 100 kilowatts.

In addition to long range weapons applications, improved visible and ultraviolet lasers would find a variety of other uses, both military and non-military. In fact, some of these uses would have much less severe performance requirements than those described above. Military applications include optical radar, remote atmospheric and meteorological measurements using Raman backscatter, and oceanographic measurements and submarine detection using wavelengths in the blue-green portion of the spectrum. Non-military applications include laser pellet fusion, isotope separation, and laser-induced chemistry.

At the present time there are no high-power, high-efficiency, visible lasers. Although they are popular in small sizes, the CW Ar^+, He-Ne and He-Cd lasers are inefficient and not scalable to large sizes. The pulsed Cu vapor and N_2 lasers are more efficient but they are difficult to scale to ARPS's requirements. The $Ar/N_2(1^+)$ and $He/N_2{}^+(1^-)$ lasers are apparently scalable (at least within the limits of high intensity electron beams), but the inefficiency is evidently limited to less than 10%. Consequently they will probably not satisfy ARPA's requirements.

Among the ideas which have been proposed, excimer lasers stand out since they offer rapid, volumetric removal of the lower laser level. The basic principle of a so-called excimer laser is illustrated in Fig. 1. The two species A and B are repulsive or, at most, weakly bound in their ground states. However, when one of them (specie A) is raised to an electronically excited state it can combine with the other species to form an excited dimer (or "excimer") AB^*. This molecule can then radiate - or lase - to the gound state, as indicated, whereupon it immediately falls apart, removing the lower laser level and assuring an inversion. Ordinarily, however, the emission is rather broadband since it corresponds to a bound-free or bound-weakly bound transition. Consequently, the simulated emission cross section is relatively small, even for allowed transitions, and enormous pumping rates are required to achieve useful gain.

To date, a number of excimer lasers have been demonstrated, as summarized in Table I, and many others have been suggested. The first excimer laser to be discovered was the Xe laser.[1-3] In theory, the Xe

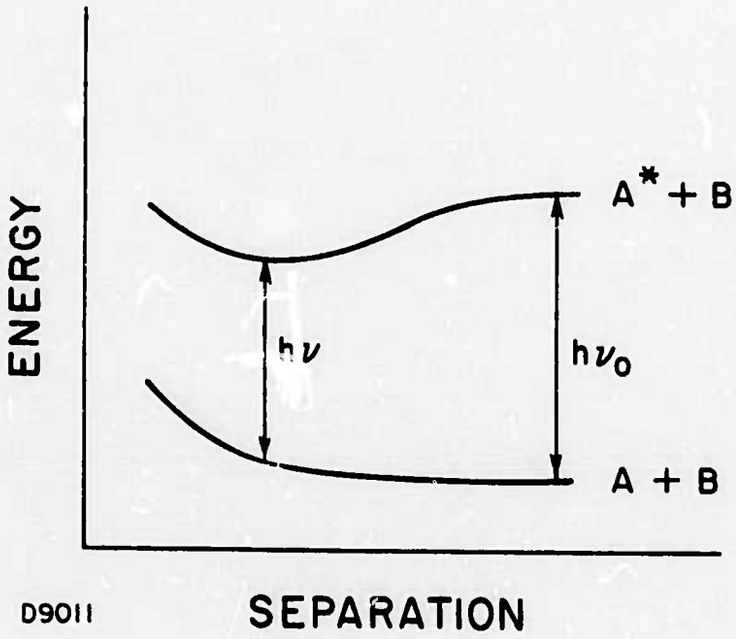

Fig. 1 Molecular Energy Level Diagram Illustrating the Principle of an Excimer Laser

excimer laser offers a high efficiency (approximately 50%) with high intensity electron beam pumping.[4] However, no more than .1% has been observed at this point.[5] The most serious drawback of this laser is the wavelength (172 nm), which is deep in the vacuum uv. At this wavelength it is difficult to find suitable windows and mirrors for high power applications. For some applications this wavelength is inconvenient because it is not transmitted by the atmosphere. The rare gas oxides, XeO and KrO, have also been shown to lase.[6] However, they require enormous pumping and appear to be limited to low efficiency.[7]

TABLE I

SUMMARY OF EXCIMER LASERS

	Species	Wavelength (nm)	Theoretical Maximum Efficiency
Demonstrated			
	Xe_2	176	50%
	Kr_2	145	
	Ar_2	126	
	XeO	540	6%
	KrO	558	
Proposed			
	XeF	354	24%
	XeBr	282	
	XeCl	308	

At the present time, the most exciting class of excimers seems to be the rare gas monohalides. The spectra of these molecules were first observed in low pressure flowing afterglows by Setser[8] and by Golde and Thrush.[9] In these experiments Cl_2 was mixed with Ar which had been previously excited by means of a microwave discharge. The rare gas halides were then formed by the reaction

$$Ar_m^* + Cl_2 \rightarrow Ar\,Cl^* + Cl, \qquad (1)$$

where Ar_m^* is a metastable state of Ar. The emission from the excited $ArCl^*$ was observed to be very bright, leading Golde and Thrush to estimate that the efficiency for producing the excited state was "more than, and possibly much more than, 10%." However, because of its short wavelength (170 nm) ArCl itself did not seem to be an interesting molecule. At this point, a theory was developed at AERL to predict the wavelengths at which the other rare gas halides should emit.[10] Subsequent experiments carried out at AERL and elsewhere[11] substantially confirm the theoretical predictions and show that several of the molecules should emit at useful wavelengths. The AERL experiments, which were carried out at relatively high pressures (up to several atmospheres), also showed very bright emission and support the idea that excited rare gas monohalides can be produced efficiently in discharges.

II. STRUCTURE OF THE RARE GAS HALIDES

A potential energy diagram showing the structure of the XeI molecule is shown in Fig. 2. It is typical of all the rare gas monohalides. At infinite internuclear separation the energy of $Xe^+ + I + e^-$ relative to Xe + I is just the ionization potential of Xe, 12.127 eV. Due to the electron affinity of I_2, 3.063 eV, the energy of $Xe^+ + I^-$ at infinite internuclear separation is 9.064 eV. As these particles approach one another they attract along a deeply descending coulomb curve which, as shown in Fig. 2, crosses all the excited states of both Xe and I and is bound by 1.3 eV (relative to $Xe + I^*$) at an internuclear separation of 2.3Å. On the other hand, the ground state of XeI is only weakly bound (XeF differs from the other monohalides in that its ground state is evidently more strongly bound). The strongest fluorescence band corresponds to the $^2\Sigma \rightarrow {}^2\Sigma$ transition at 254 nm. This is an allowed transition with a lifetime estimated to be $\lesssim$ 100 ns. This band is also the narrowest of the fluorescence bands since it corresponds to a bound-weakly bound transition. Since the lower level is split into Σ and Π branches broad, red-shifted bands appear at approximately 325 and 360 nanometers, corresponding to the $^2\Sigma \rightarrow {}^2\Pi$ transitions. Although it is not shown in Fig. 2, the upper level is split in a manner similar to the lower level. This is because the Xe^+ ion has a ^2P configuration similar to the ground state of the I atom. In the case of the Xe^+ ion, the $^2P_{1/2}$ state lies approximately 1 eV above the $^2P_{3/2}$ ground state. The $^2\Pi$ levels which

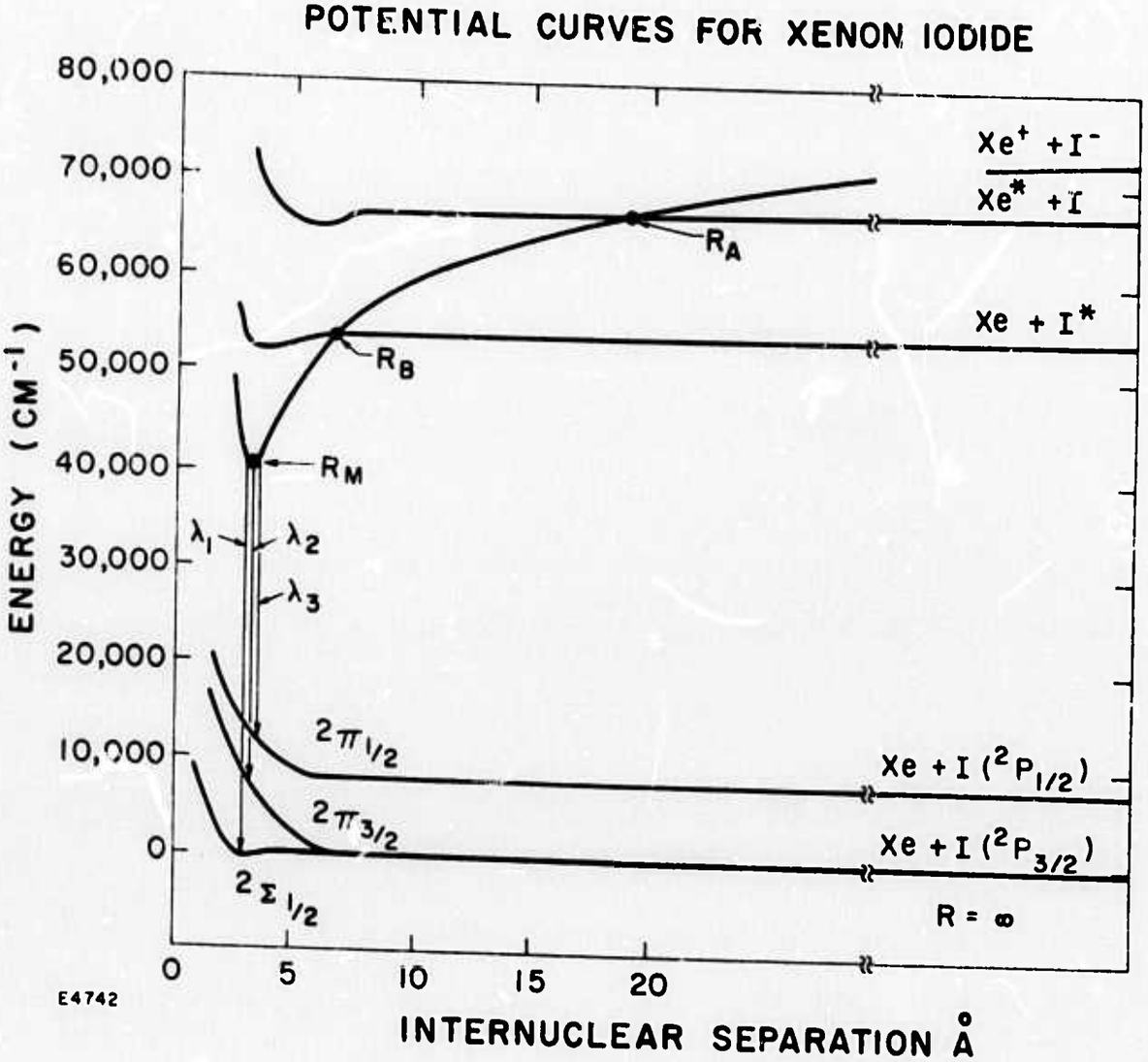

Fig. 2 Potential Energy Diagram Showing the Structure of Xenon Iodide

arise from this splitting lead to emission which is blue shifted from the $^2\Sigma \rightarrow {}^2\Sigma$ transition. This emission has been observed weakly in XeF. To provide a qualitative description of the structure of these molecules a theory has been developed at AERL which is based on the analogy between these molecules and the alkali halides[10] (see Appendix A). According to this theory, the excited rare gas atom is likened to an alkali atom. This is justified by the fact that both species have a single s electron outside an ionic core with about a 4 eV ionization potential. The theoretical predictions are therefore based on the structure of the nearest alkali halide. For example, the structure of XeI is like that of CsI. A table of the predictions made from this model is shown in Table II. At the time when this table was constructed, the only data available were for ArCl. Subsequently, the predictions of the theory have been confirmed from a number of molecules at AERL and elsewhere. It is also evident from the table that several species have emission bands at interesting wavelengths.

TABLE II

PREDICTED FEATURES OF INERT GAS MONOHALIDES

(Observed wavelengths shown in parenthteses)

Molecule	$R_M(\mathring{A})$	$E_M(cm^{-1})$	λ_1(nm)	λ_2(nm)	λ_3(nm)
XeI	3.3	39135	256(254)	302	342
XeBr	3.1	34272	292(282)	354	407
XeCℓ	2.9	30860	324(308)	402	417
XeF	2.35	25195	397(353)	521	532
KrI	3.2	54000	185	208	247
KrBr	2.9	49353	203	231	252
KrCℓ	2.8	45592	219	253	258
KrF	2.27	39229	256	301	305
ArBr	2.8	62152	161	178	190
ArCℓ	2.7	58042	172(170)	192	195
ArF	2.17	37484	267	318	322
NeF	1.93	93266	107	115	115

For ArI, NeI, NeBr and NeCℓ and the helium halides the inert gas ionization potential is so large that the coulomb curve does not make up sufficient energy to approach the low lying halogen excited states. These compounds should only have small well depths and the molecular continua should be near the free atom lines. Possibly ionic states of the opposite polarity, viz. Ne^- and I^+, could enter into the binding.

III. EXPERIMENTAL APPARATUS

The experimental results observed at AERL were obtained with a high-intensity electron beam which was used to pump high pressure mixtures of Ar, Xe and the halogens. The electron beam gun is shown in Figs. 3 and 4. The electron beam produced by this gun has an energy of approximately 400 keV per electron, and an intensity of about 30 A/cm^2 passing through the foil, over an area of approximately 1 cm by 15 cm. For laser experiments the intensity is increased to about 150 A/cm^2 through the foil at the expense of lowering the energy to about 300 keV per electron. The duration of the electron beam pulse is approximately 100 ns, with a 10 ns rise time and a 20 ns fall time. The gun has proved to be very reliable, and dozens or hundreds of shots are generally obtained between foil failures.

The cell is mounted directly on the electron beam gun as shown in Fig. 4. Several cells are available, including stainless steel cells with brazed sapphire windows capable of operating at temperatures up to 900°F and pressures up to 100 psia. In the present experiment an aluminum cell is used which is compatible with fluorine. The valves are stainless steel and the windows are sapphire or quartz. For maximum reliability, a .001 in stainless steel foil is generally used. Titanium is corroded by the haologens and aluminum is not as strong as stainless steel. However, for maximum electron beam transmission, aluminized kapton films are used. The cell can be warmed up using built-in cartridge

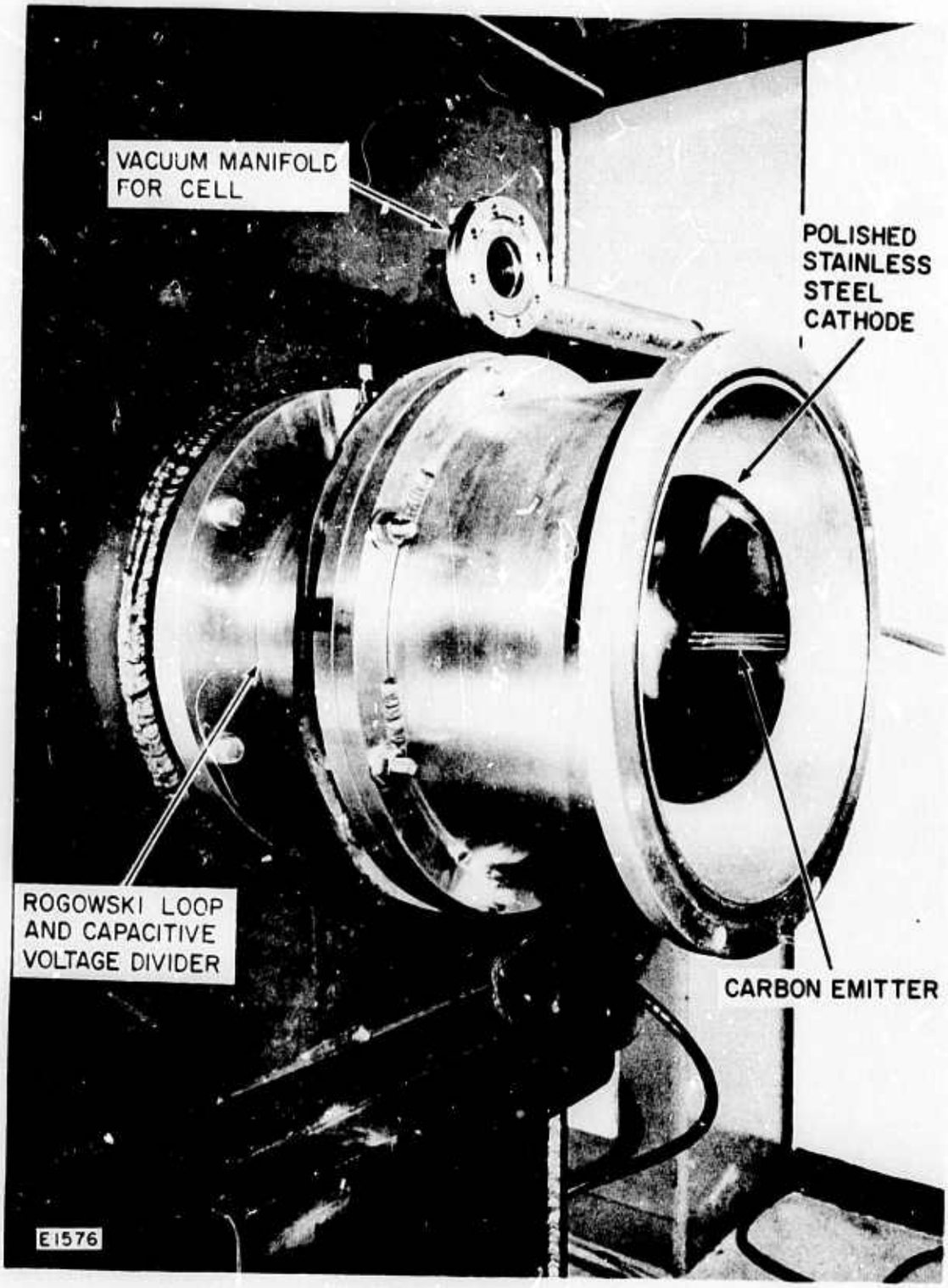

Fig. 3 Photograph of the AERL High Intensity Electron Beam Gun

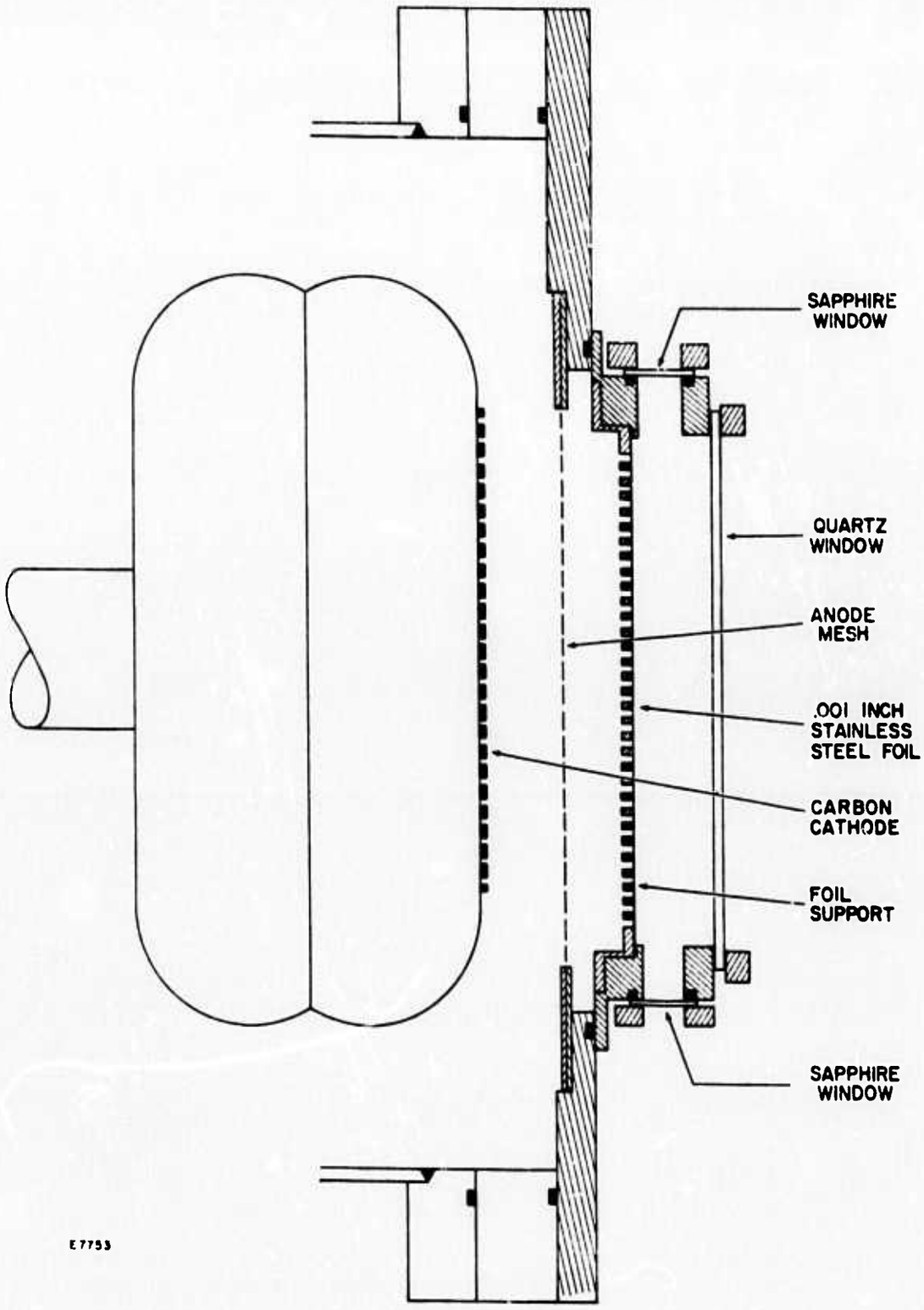

Fig. 4 Cross-Sectional View of the High Intensity Electron Beam Gun and Laser Cell

heaters to provide a mild bake-out. The cell can be pumped out to an ultimate vacuum of better than 10^{-5} torr with a leak rate better than 10^{-4} torr/hr. Therefore, purity is not a problem.

The gases, except I_2 vapor, are premixed in stainless steel tanks and allowed to stand for several hours, or even several days, to assure that they are fully mixed when they are used. The iodine crystals were obtained from Merck and are claimed to be >99% pure. They were placed in a small stainless steel sample cylinder attached to the cell through a stainless steel valve. The crystals and sample cylinder were repeatedly allowed to outgas at room temperature (under vacuum but valved off) and then cooled with liquid N_2 snd pumped out. The I_2 vapor is introduced directly into the evacuated cell and allowed to come into equilibrium. The rare gases are then admitted to the desired pressure and allowed to mix. Mixing is occasionally stimulated by firing the electron beam gun to warm the gas in the irradiated region. The liquid bromine was similarly outgassed by repeated freeze, pump, thaw cycles. Prior to making the measurements with F_2, the cell and mixing manifold were passivated by filling them with an F_2-rich mixture at low pressure (a few torr to half an atmosphere) for several hours.

The diagnostics, shown in Fig. 5, include time-integrated and time-resolved emission measurements, as well as laser absorption measurements. The time-integrated emission measurements are made with quarter-meter and half-meter Hilger quartz prism instruments, using film. Generally, at high pressures, one shot is sufficient to provide a medium resolution spectrum using 50 μm slits. This corresponds

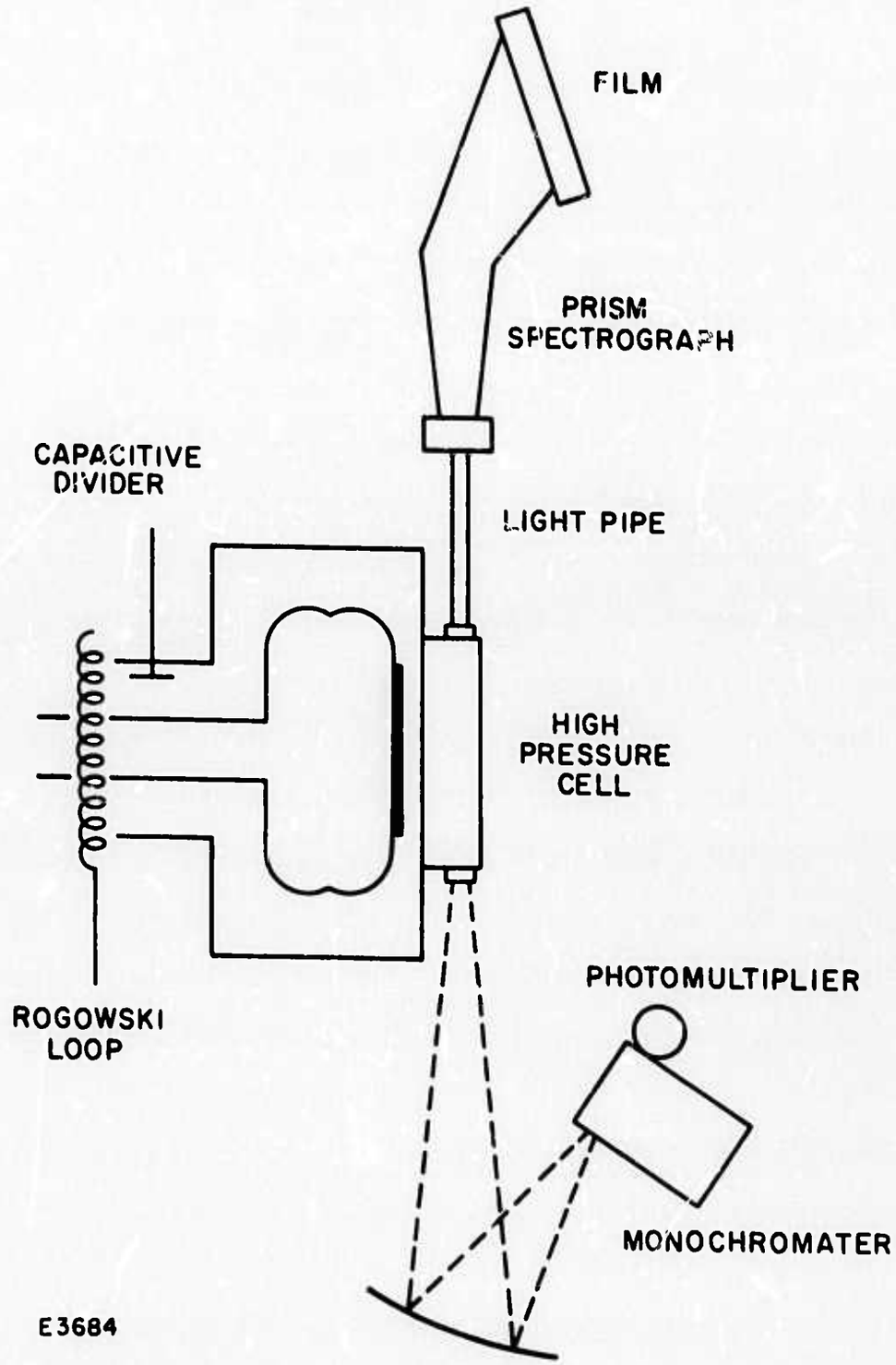

Fig. 5 Schematic Diagram of Emission Diagnostics for Fluorescence Experiments

to a wavelength resolution of approximately .1 nm. The time-resolved emission measurements are made with a Jarrel-Ash one-quarter meter f/3.5 Ebert monochromater with a 1P28 photomultiplier tube, and Tektronix 551 oscilloscopes with type K and L preamps. The spectral resolution of this system is about .1 nm. The time resolution is limited by the oscilloscopes to approximately 10 ns. To provide an adequate signal/noise ratio, it has been found necessary to provide adequate lead shielding around the photomultiplier to screen out X-rays. In addition, it has been necessary to place the oscilloscopes in a screen room and provide careful grounding and shielding of the photomultiplier. Because of the intense emission observed from the rare gas halides it has been found necessary to take extreme care to prevent saturation of the photomultiplier. Laser absorption measurements have been made using a CW argon ion laser to measure I_2 absorption and a CW helium-cadmium laser operating at 325 nm to observe Cl^- absorption.

Finally, laser optics and alignment equipment are available for laser experiments. The optical cavity consists of two high reflectivity mirrors separated by about 25 cm. A stable resonator configuration is used in which one mirror has a 1 m radius of curvature and the other is flat. To reduce the losses, the normal incidence windows are aligned with the cavity. The alignment is carried out with a Davidson Optronics alignment telescope. Alignment accuracy of about .1 mrad is easily achieved, although much larger misalignments have no observable effect on the results.

IV. EXPERIMENTAL RESULTS

Some results of the time-integrated spectral measurements are shown in Figs. 6 through 10. In the XeI spectrum, Fig. 6, we see the $^2\Sigma \rightarrow {}^2\Sigma$ transition sharply peaked at about 254 nm, and shading off toward the blue with little structure. The broad, smooth $^2\Sigma \rightarrow {}^2\Pi$ transitions are also evident at 325 and 360 nm. In the XeBr spectrum, Fig. 7, we see the $^2\Sigma \rightarrow {}^2\Sigma$ band sharply peaked at 282 nm. This band shades off toward the blue with a diffuse vibrational structure superimposed on the continuum. In the XeC spectrum, Fig. 8, the $^2\Sigma \rightarrow {}^2\Sigma$ band peaks at 308 nm, and shades off toward the blue with a sharper vibrational structure. From the separation of the vibration peaks we find that the vibrational spacing is approximately 210 cm^{-1}. Since the vibrational spacing in cesium chloride is 209 cm^{-1}, this provides strong support for alkali halide model. The $^2\Sigma \rightarrow {}^2\Sigma$ band of the XeF molecule, shown in Figs. 9 and 10 peaks near 353 nm and shades off toward the blue. Although the broad structure of this band is similar to that of the $^2\Sigma \rightarrow {}^2\Sigma$ bands of the other molecules, much more structure is evident. This is to be expected since XeF_2, XeF_4 and XeF_6 are observed to be stable at room temperature.[12] Moreover, the predicted wavelength shown in Table II is too long for XeF. The shift corresponds to about 3000 cm^{-1}. This is less than the bond strength of XeF which is estimated to be between 3500 and 7000 cm^{-1}. The difference can be accounted for by assuming that the transition takes place to a high vibrational level of

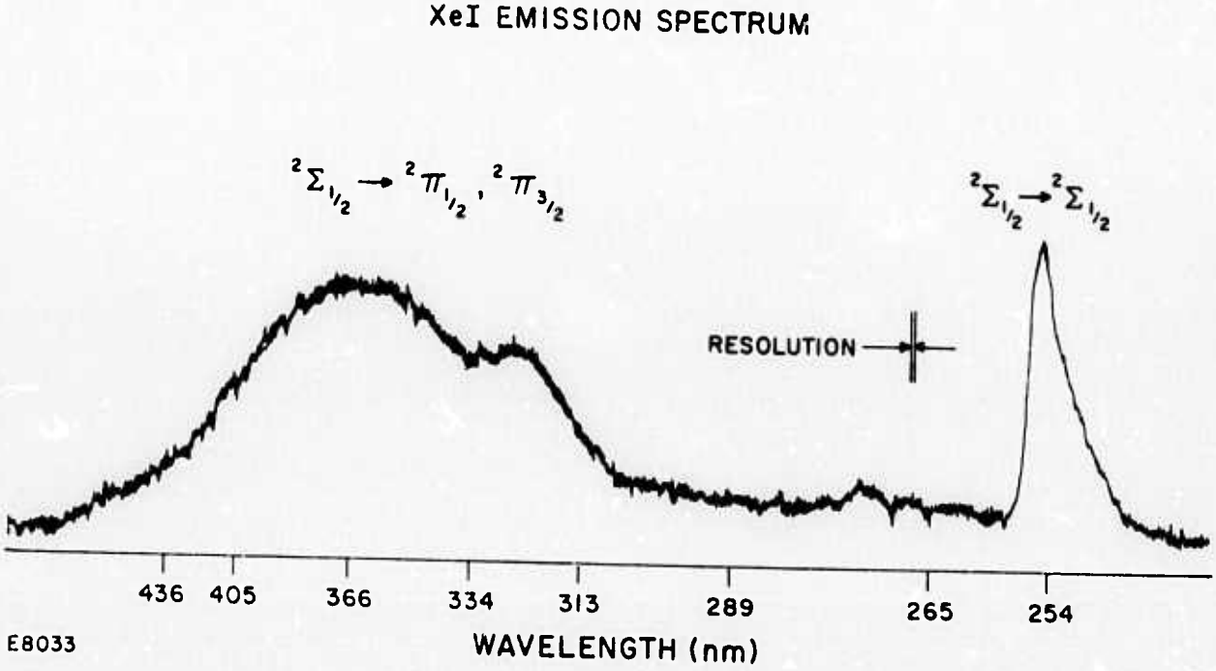

Fig. 6 Densitometer Trace of XeI Emission Spectrum

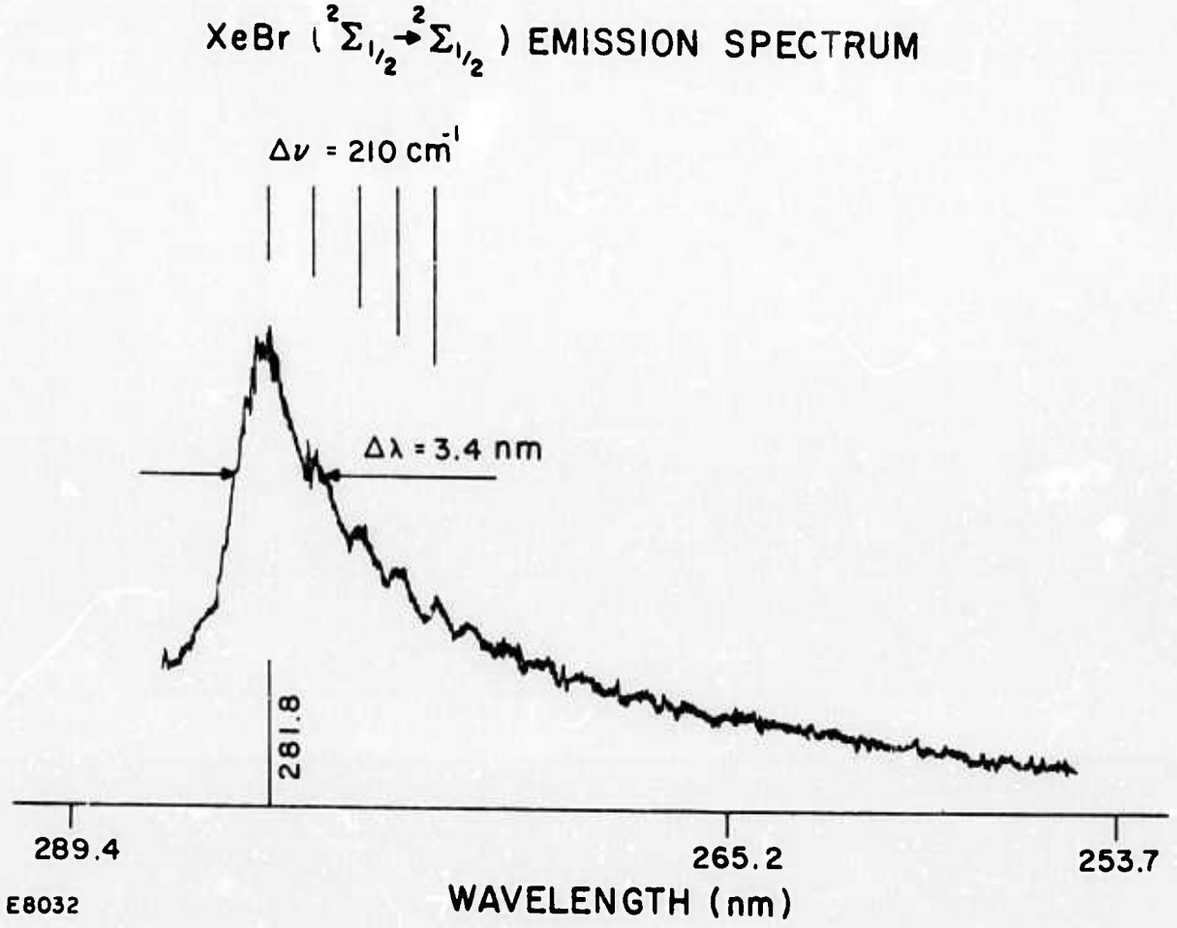

Fig. 7 Densitometer Trace of XeBr ($^2\Sigma \rightarrow {}^2\Sigma$) Emission Spectrum

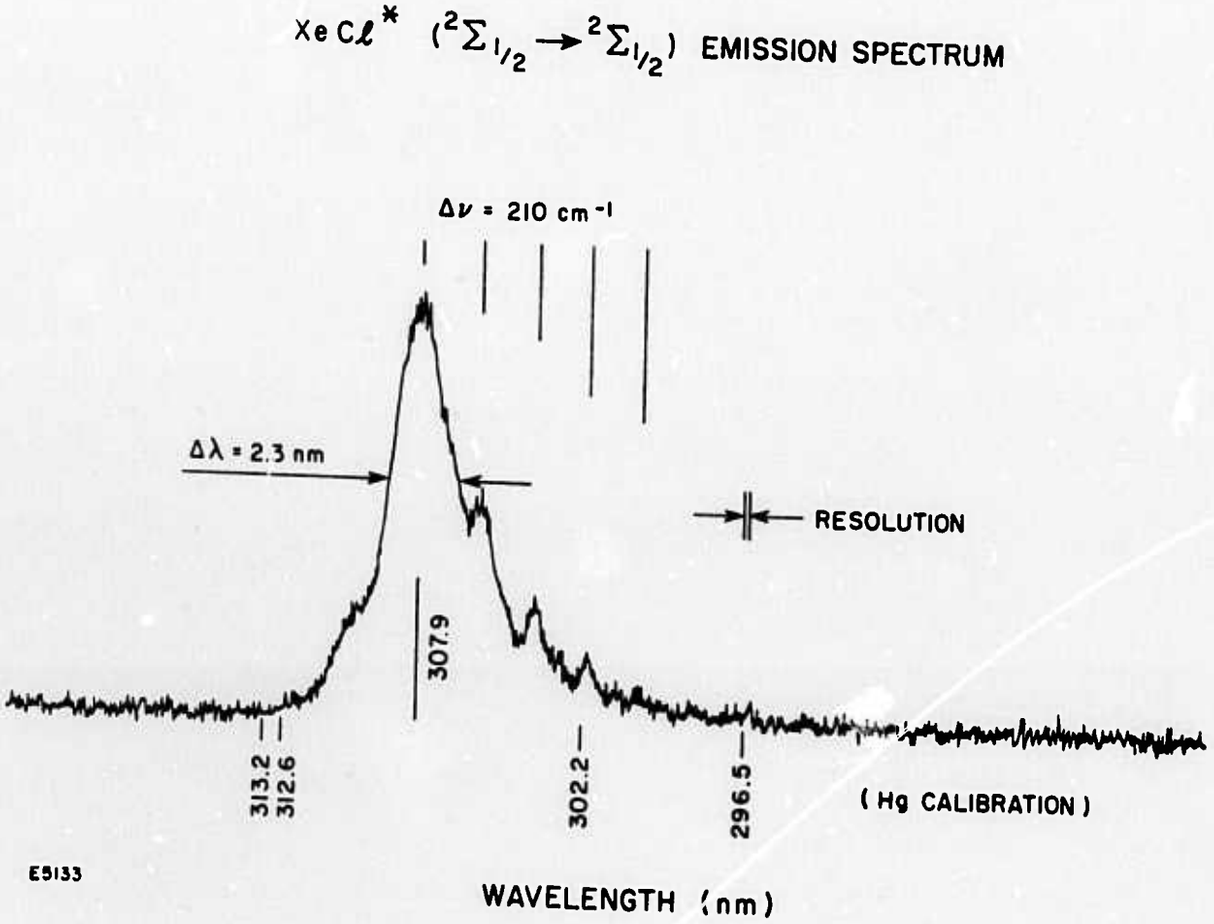

Fig. 8 Densitometer Trace of XeCl ($^2\Sigma \rightarrow {}^2\Sigma$) Emission Spectrum

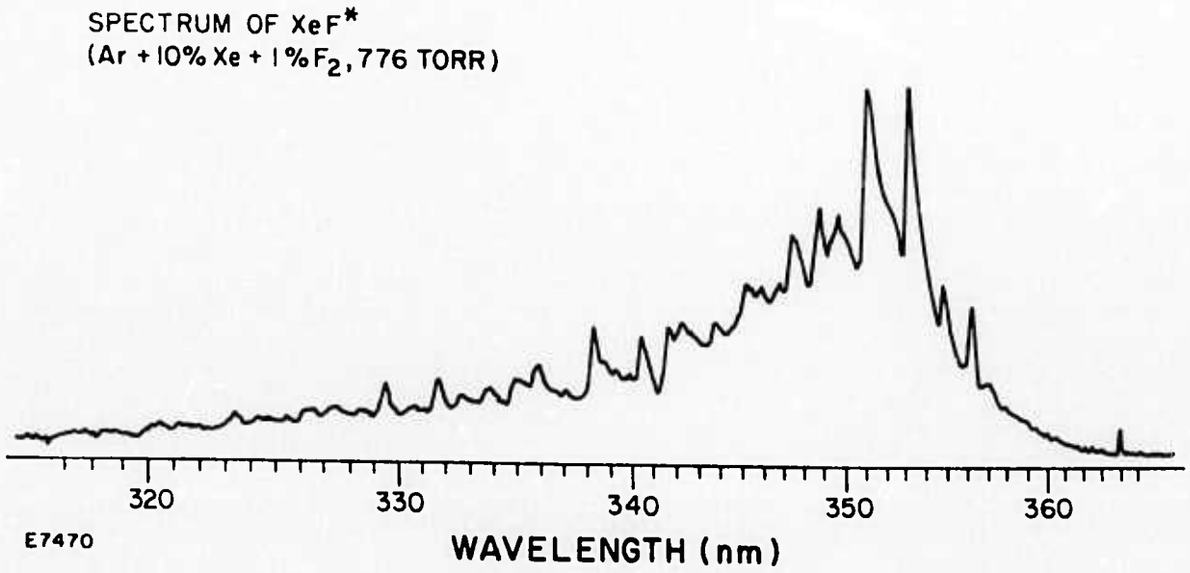

Fig. 9 Densitometer Trace of XeF ($^2\Sigma \rightarrow {}^2\Sigma$) Emission Spectrum

the ground electronic state, as shown in Fig. 11. Further support for this conjecture comes from what is known, or can be estimated, regarding the bond lengths of the upper and lower electronic states. According to the alkali halide model, the bond length in the upper state should be about 2.3 Å, whereas the observed bond length in XeF_2 is 2.0 Å.[21] Because of its complexity, the vibrational structure of the XeF ($^2\Sigma \rightarrow {}^2\Sigma$) band emission is difficult to analyze. There appear to be two series of vibrational lines in XeF spectrum. Each series has a spacing of about 300 cm^{-1} and the two series are displaced with respect to each other by about 160 cm^{-1}. The conjecture is that the 300 cm^{-1} spacing represents the vibrational spacing of the excited XeF, while the 160 cm^{-1} spacing represents the vibrational spacing in the upper levels of the ground electronic state. The vibrational spacing in CsF is 365 cm^{-1} and the vibrational spacing in electronically excited XeF should be about the same, in fair agreement with the observed 300 cm^{-1} spacing. The vibrational level spacing of the $XeF_2(\nu_3)$ (asymmetric stretch) mode is 560 cm^{-1}.[12] However, the bond strength of XeF is expected to be quite a bit smaller and therefore the vibrational frequency should be correspondingly smaller. Thus, the low value of the vibrational spacing in the ground electronic state may be accounted for by the relatively weak bond strength in XeF compared to XeF_2, and the high vibrational level to which the fluorescence takes place. The observed width of the vibrational peaks in the XeF spectrum is due to unresolved rotational structure. A theoretical rotational band profile corresponding to a single vibrational transition has been constructed using the estimated bond lengths for the upper and

lower levels. Typically, near the center of the rotational band, the individual rotational lines are separated by approximately .4 cm^{-1}. The pressure width of these lines at 1 atm is estimated to be approximately .03 cm^{-1}, which is small compared to the rotational line spacing. However, the individual rotational levels will be split into six spin-orbit components. If the spin-orbit splitting is large compared to the pressure width of the lines, the resulting spectrum will be essentially a continuum. To estimate the stimulated emission cross section it will be assumed that the rotational band may be approximated by a structureless continuum. If the spin-orbit splitting is small compared with the pressure width of the rotational lines there will be spaces between the lines and the gain at the peak of the lines will be larger. Consequently, the gain calculated on the basis of a continuous rotation band provides a lower limit to the gain which might be expected.

A potential difficulty of the XeF system is the possibility of bottlenecking in the lower laser level. If the bond energy in the lower laser level is much greater than the temperature, dissociation from the lower laser level will not take place. On the other hand, if the emission takes place to a high vibrational level of the lower electronic state, vibrational relaxation to lower level vibrational levels may prevent bottlenecking. Using the semiempirical theory of Milikan and White[13] the relaxation time is estimated to be approximately 30 ns-atm for collisions with argon atoms. The vibrational relaxation time may be shorter than this if vibration-rotation interaction is important. In fact, rotational relaxation itself may help relieve the bottlenecking problem.

Some spectra of XeF obtained at lower pressures are shown in Fig. 10. At lower pressures the spectra become spread out towards the blue due to incomplete relaxation of the upper electronic state prior to emission. The upper state seems to be completely relaxed at pressures greater than approximately .5 atm. However, there is no evidence regarding the relaxation of the lower level. In addition to the $^2\Sigma \rightarrow {}^2\Sigma$ transition at 353 nanometers, another structured band appears at about 264 nm. This is due to the $^2\Pi \rightarrow {}^2\Sigma$ transition originating from the state which correlates with the $Xe^+(^2P_{1/2})$ state. There is also a broad smooth continuum centered near 450 nm which becomes relatively stronger at low pressures. The origin of the pressure dependence is not known, but it would seem to indicate that the band does not originate from the same upper level as the 353 nm band, and is, therefore, not the $^2\Sigma \rightarrow {}^2\Pi$ band.

Time-resolved emission measurements have been made on XeF using both Xe/F_2 mixtures and $Ar/Xe/F_2$ mixtures. The measurements span a pressure range between 2 torr and 6 atm, and F_2 concentrations between 10^{-3}% and 3%. At high pressures the emission is observed to rise rapidly and decay rapidly when the beam turns off. This suggests that the XeF is formed by very rapid processes. In addition, the lifetime of the excited state of XeF has been measured in Xe/F_2 mixtures. Some typical data are shown in Fig. 11. When the decay times derived from such data are plotted versus the pressure, the natural lifetime and the quenching rate may be determined as shown in Fig. 12. On the basis of these data the radiative lifetime τ_ν is found to be approximately 50 ns, and the rate

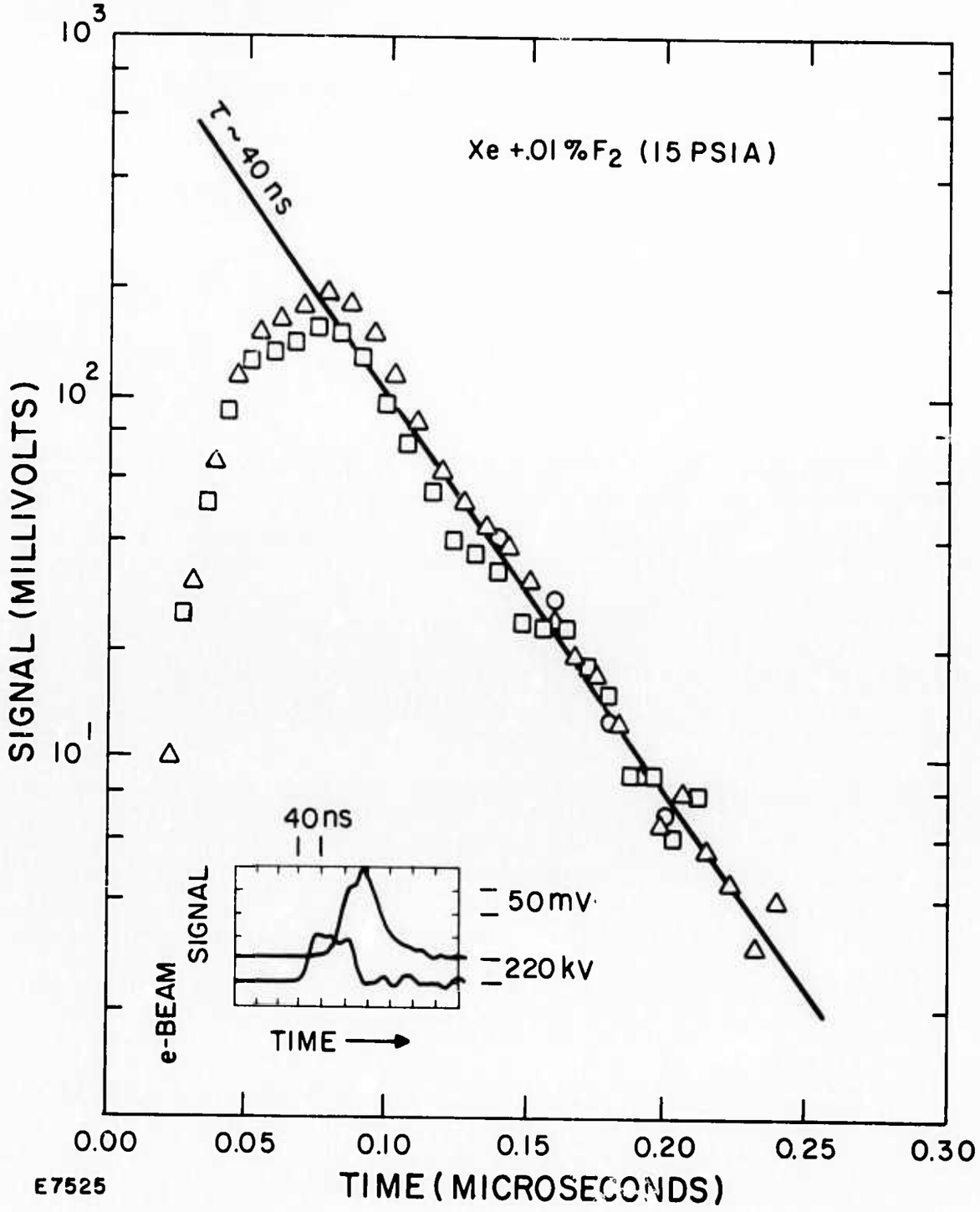

Fig. 11 Decay of XeF Emission in E-beam Excited Mixtures of F_2 in Xe

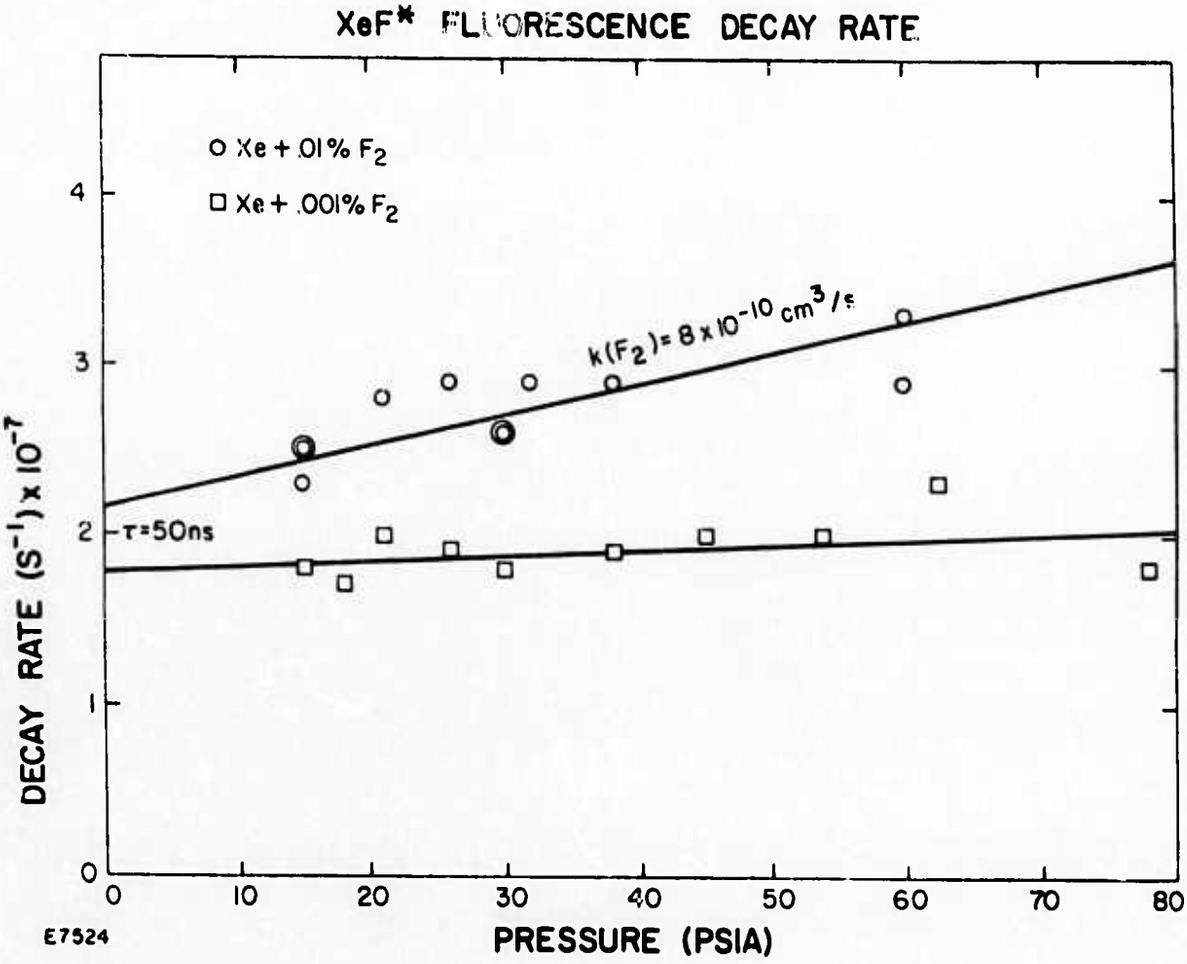

Fig. 12 Decay Rate for XeF Emission in e-beam Excited Mixtures of F_2 in Xe

coefficient k_Q for the quenching of excited XeF by F_2 is found to be 8×10^{-9} cm^3/s. There is no evidence of significant quenching of excited XeF by Xe. For these measurements the electron beam was attenuated by approximately a factor of 30 to keep the electron concentration below approximately $10^{13}/cm^3$. Under these conditions quenching by electrons should be insignificant.

In addition to these emission measurements, laser absorption measurements have been made on mixtures of Xe and $C\ell_2$ to detect the presence of $C\ell^-$ ions. For these purposes a CW helium-cadmium laser was used, with a wavelength of 325 nm. At this wavelength the absorption cross section of $C\ell_2$ is 2.5×10^{-19} cm^2. [14] The photodetachment cross section of $C\ell^-$ at this wavelength is 1.8×10^{-17} cm^2. [15] When a mixture of Ar, Xe and $C\ell_2$ is excited by the electron beam, no increase in the absorption is observed. In fact, under some circumstances a slight decrease of the absorption appears. This implies that there is no significant absorption by $C\ell^-$ ions. Evidently these ions are rapidly consumed by the Thompson recombination process

$$C\ell^- + Xe^+ M \rightarrow XeC\ell^* + M \qquad (2)$$

where M is any third body. Processes of this type have been observed for other species and are generally quite fast, having a recombination coefficient of the order of 2×10^{-25} cm^6/s. [16]

V. KINETICS

These results may be interpreted in terms of the reactions shown in Table III. The pumping reactions are similar to those discussed by SRI[17, 18] and are presumed to be well understood. The formation of excited XeF^* is assumed to take place via two paths. In the first path, the excited Xe^* atoms react with F_2 molecules to produce excited XeF^*, or possibly ground state De plus two F atoms (reaction 19). The branching ratio is not known and should be determined as soon as possible by making absolute fluorescence measurements. The second mechanism for forming excited XeF^* consists of dissociative attachment of electrons to F_2 molecules (reaction 17), followed by three-body Thompson recombination of F^- ions with Xe^+ ions to form exited XeF^* molecules (reaction 23). As indicated in the table, this latter reaction is extremely fast. Since the first step is rate limiting and is two-body in order, this mechanism should dominate at low pressures since it does not depend upon the relatively slow three-body recombination of atomic ions to form molecule ions (reactions 3 and 9) from which excited atoms are in turn formed by dissociative recombination (reactions 4 and 10). The excited XeF molecules are lost by radiative decay, quenching by F_2 and, perhaps, quenching by electrons. There is no direct evidence regarding the rate of quenching of XeF by electrons (reaction 28), and a rate coefficient of 2×10^{-8} cm^3/s has been used. At sufficiently high partial pressures of Xe, the excited Xe^* atoms will tend to dimerize to

TABLE III

ARGON/XENON/FLUORINE KINETICS

Reaction			Rate Coefficient
Pumping reactions:			
1. $\vec{e} + Ar$	$\rightarrow$	$\vec{e} + Ar^*$	6.5×10^{16}/J
2. $\vec{e} + Ar$	$\rightarrow$	$\vec{e} + Ar^+ + e^-$	2.4×10^{17}/J
3. $Ar^+ + Ar + M$	$\rightarrow$	$Ar_2^+ + M$	2.5×10^{-31} cm^6/s
4. $Ar_2^+ + e^-$	$\rightarrow$	$Ar^* + Ar$	$3.3 \times 10^{-5} T_e^{-.67}$ cm^3/s
5. $Ar^* + Ar + M$	$\rightarrow$	$Ar_2^* + M$	8.3×10^{-33} cm^6/s
6. $Ar^* + Ar$	$\rightarrow$	Ar_2^*	1.7×10^{-15} cm^3/s
7. $\vec{e} + Xe$	$\rightarrow$	$\vec{e} + Xe^*$	1.3×10^{17}/J
8. $\vec{e} + Xe$	$\rightarrow$	$\vec{e} + Xe^+ + e^-$	2.9×10^{17}/J
9. $Xe^+ + Xe + M$	$\rightarrow$	$Xe_2^+ + M$	2×10^{-31} cm^6/s
10. $Xe_2^+ + e^-$	$\rightarrow$	$Xe^* + Xe$	$2.4 \times 10^{-5} T_e^{-1/2}$ cm^3/s
11. $Xe^* + Xe + M$	$\rightarrow$	$Xe_2^* + M$	2.5×10^{-32} cm^6/s
12. $Xe^* + Xe$	$\rightarrow$	Xe_2^*	2.3×10^{-13} cm^6/s
13. $Ar^* + Xe$	$\rightarrow$	$Ar + Xe^*$	2.1×10^{-10} cm^3/s
14. $Ar_2^* + Xe$	$\rightarrow$	$2Ar + Xe^*$	1×10^{-9} cm^3/s
15. $Ar^+ + Xe$	$\rightarrow$	$Ar + Xe^+$	0 (?)
16. $Ar_2^+ + Xe$	$\rightarrow$	$2Ar + Xe^+$	0 (?)
17. $e^- + F_2$	$\rightarrow$	$F^- + F$	$6 \times 10^{-8} T_e^{-.34}$ cm^3/s
Excitation reactions:			
18. $Xe^* + F_2$	$\rightarrow$	$XeF^* + F$	6×10^{-10} cm^3/s
19. $Xe_2^* + F_2$	$\rightarrow$	$Xe + 2F$	0 (?)

TABLE III (cont.)

ARGON/XENON/FLUORINE KINETICS

Reaction			Rate Coefficient
20. $Xe_2^* + F_2$	→	$XeF^* + F + Xe$	6×10^{-10} cm^3/s
21. $Xe_2^* + F_2$	→	$Xe + 2F + Xe$	0 (?)
22. $Xe^+ + F^-$	→	$Xe^* + F$	3×10^{-7} cm^3/s
23. $Xe^+ + F^- + M$	→	$XeF^* + M$	2×10^{-25} cm^3/s
24. $Xe_2^+ + F^-$	→	$Xe_2^* + F$	3×10^{-7} cm^3/s
25. $Xe_2^+ + F^- + M$	→	$XeF^* + F + M$	2×10^{-25} cm^3/s
Loss reactions:			
26. XeF^*	→	$XeF + h\nu$	2×10^7/s
27. $XeF^* + F_2$	→	$XeF + F + F$	8×10^{-10} cm^3/s
28. $XeF^* + e^-$	→	$XeF + e^-$	2×10^{-8} cm^3/s
29. Xe_2^*	→	$Xe + Xe + h\nu$	4×10^7/s
30. Ar_2^*	→	$Ar + Ar + h\nu$	3.1×10^7/s
31. $Xe^* + Xe^*$	→	$Xe_2^+ + e^-$	5×10^{-10} cm^3/s
32. $Xe^* + Xe_2^*$	→	$Xe_2^+ + Xe + e^-$	5×10^{-10} cm^3/s
33. $Xe_2^* + Xe_2^*$	→	$Xe_2^+ + 2Xe + e^-$	5×10^{-10} cm^3/s
34. $Xe^* + XeF^*$	→	$Xe_2^+ + F + e^-$	5×10^{-10} cm^3/s
35. $Xe_2^* + XeF^*$	→	$Xe_2^+ + XeF + e^-$	5×10^{-10} cm^3/s

form Xe_2^* molecules. This represents a loss mechanism since the Xe_2^* molecules can radiate before they react with the F_2. A further loss mechanism is provided by Penning ionization, reactions 31-35. However, at the excited state densities anticipated for rate gas halide systems this loss mechanism should not be too important, except insofar as it controls the ionization rate in a discharge.

VI. CONCLUSIONS

On the basis of these results a number of remarks can be made regarding the laser potential of the rare gas halides. From the observed lifetime (50 nanoseconds) and bandwidth (1.5 nanometers) of excited XeF we find that the stimulated emission cross section is approximately

$$\sigma_{stim} = \frac{1}{4\pi}\sqrt{\frac{\ell n 2}{\pi}}\frac{\lambda^3}{c\tau_\nu}\frac{\lambda}{\Delta\lambda} = 2.6\ \text{Å}^2 \qquad (3)$$

Assuming that the radiative lifetimes of the other rare gas halides are comparable, the stimulated emission cross sections will probably be a bit smaller. This is partly because they emit at shorter wavelengths. However, the most important factor is the larger bandwidth which results because the lower level is only weakly bound.

In order to produce laser action one not only needs an inversion but also must have the total net gain be greater than any intrinsic losses in the laser gas mixture. This section describes the loss mechanisms appropriate to these molecules. There are four basic sources of loss which can be present in an inert gas/halogen mixture being excited by either an e-beam or a discharge. First, the parent halogen, F_2, $C\ell_2$, Br_2 or I_2, can absorb. Second, the excited species initially produced can absorb. These are the parent inert gas metastables, Ar^*, Kr^*, Xe^*..., or their corresponding molecular excimer states, Ar_2^*, Kr_2^*, Xe_2^*.... These molecules can absorb in both the visible and in the uv. The atomic uv

photoionization continua are the most important for our considerations here. Third, any ions produced such as Ar_2^+ or Xe_2^+ or halide negative ions can absorb in the visible and in the uv. However, the steady-state densities of these species can be kept low. Finally, the noble gas monohalides can exhibit loss themselves by having an overlapping absorption band. We have made estimates of the loss mechanisms for all of the inert gas monohalides.

The self-absorption bands of the XeX^* are very similar in nature to the emission bands used for lasing. For example, the lasing bands in XeF take the excited ion pair molecule Xe^+F^- to a low lying covalent state of XeF:

$$Xe^+F^- \rightarrow XeF + h\nu\ (3535\ \mathring{A}). \tag{4}$$

The covalent molecular wavefunctions for XeF ground state look essentially like the product of ground state free-atom wavefunctions. The possible competing absorption process of Xe^+F^- would be one in which the photo would transfer the electron from F^- into a higher lying excited orbital of Xe^*, making a molecule whose wavefunction is more like a product of Xe^* and F atomic wavefunctions. This absorption by the excited state can be presented by the reaction

$$h\nu + Xe^+F \rightarrow Xe^* + F. \tag{5}$$

An estimate of the energetic accessibility of such a process can be made by assuming the Xe^* + F potential is not strongly dependent on

the internuclear separation, while the shape of the ionic potential curve is known from the analogous alkali halide. Absorption of this type can severely limit the laser efficiency if its cross section is comparable to the stimulated emission cross section. Of course, if it is larger it will prohibit lasing altogether. This type of absorption is energetically possible for all of the $^2\Sigma \rightarrow {}^2\Sigma$ transitions except those in XeF, ArF, KrF and maybe XeCℓ. Its impact on overall laser efficiency needs to be determined.

The absorption loss due to the halogens is a problem only for the $^2\Sigma \rightarrow {}^2\Sigma$ band of XeCℓ, but not in any other case. The Br_2 absorption band overlaps slightly the low gain $^2\Sigma \rightarrow {}^2\Pi$ transition in that molecule. The loss due to $C\ell_2$ absorption at the center of the XeCℓ $^2\Sigma \rightarrow {}^2\Sigma$ band will be about 2% cm^{-1} for $C\ell_2$ densities of $10^{17}/cm^3$. Alternatively, a different Cℓ source could be used to avoid halogen absorption problems.

Loss by negative ions could also be a problem for many of these molecules since the X^- absorption typically has threshold in the 4000-3000 Å region. The cross sections for X^- absorption increase in the sequence $\sigma(F^-) < \sigma(C\ell^-) < \sigma(Br^-) < \sigma(I^-)$. This possible loss mechanism is dramatically diminished in importance by the rapid three-body ion recombination reactions typified by reaction (3), above. For a very large ion production rate of 10^{23} ions/cm^3-s and buffer gas densities of $2 \times 10^{19}/cm^3$, and a three-body recombination rate constant of 10^{-25} cm^6/s, the halide ion number density will be only $2 \times 10^{14}/cm^3$. For the worst possible case this will lead to an absorption of less than 1/2% cm^{-1}. Since discharge pumped lasers will have ion production

rates somewhat lower than $10^{23}/cm^3$-s, negative ion photodetachment absorption should not be a problem.

Loss by positive ions such as Xe_2^+ or Ar_2^+ is harder to estimate because the size of the transition moments and the location of such ion bands is not known. Again, as in the case of the halide negative ions, the densities of these species are kept low by rapid termolecular ion-ion recombination and dissociative ion-electron recombination. Assuming that the positive ions have a broad, continuous absorption band at the right wavelength, positive molecule ion absorption should not be a problem, even with an oscillator strength of . 1.

Loss by inert gas excited states, either in the atomic form, such as Xe^* or Ar^*, or in the molecular form, such as Xe_2^* or Ar_2^* are the final important loss mechanisms. By working with gas mixtures in which the Xe is diluted in Ar, one can kinetically limit the amount of Xe_2^* formed in a discharge or an e-beam pumped xenon halide laser. Analogously, Kr/A mixes or Ar/Ne mixes would be ideal for producing krypton or argon halide lasers. In the xenon halide system, the density of the excimers of the host, Ar_2^* is kept low by having these species transfer rapidly to the xenon. Since processes like $Ar_2^* + Xe \rightarrow Xe^* + 2Ar$ have exceptionally large cross sections, with corresponding rate constants of the order of 10^{-8} cm^3/s, the steady-state density of Ar_2^* for $[Xe] \approx 10^{17}/cm^3$ and pumping rates of 10^{23} excitations/cm^3-s will be $[Ar_2^*] \approx 10^{14}/cm^3$. Even with very large absorption cross section, the Ar excimer density is too low to cause significant absorption. In mixtures of pure Xe with small amounts of halogen, Xe_2^* excimers can form an

absorb. This, briefly, is one reason for working with mixtures dilute in argon. In the absence of large excimer densities, one can still have losses due to the atomic excited states, Ar^* and Xe^*. If the laser transition of interest is at longer wavelengths than the photoionization limit of Ar^* or Xe^*, absorption can only be on discrete atomic transitions. Such transitions have very large cross sections, but they occur in very small, narrow spectral regions. This is the case for XeF, and losses due to atomic absorption should be of only minor importance. For species like XeBr which have shorter wavelengths for the brightest bands, the molecular emission spectrum will be overlapped by absorption due to photoionization of the metastable Xe^*. This overlapping band will be present for all of the $^2\Sigma \rightarrow {}^2\Sigma$ bands except that in XeF. The cross section for photoionization will at worst be 10^{-17} cm^2. Since a safe assumption is that $[Xe^*] \approx [XeX^*]$, unless the quenching of XeX^* by X_2 is very slow, we see that a stimulated emission cross section $\sigma(XeX) > 10^{-17}$ cm^2 is desirable to minimize photoionization losses.

In summary, the best candidate (on paper) is XeF since it does not have self-absorption, Xe^* photoionization absorption or F_2 absorption problems. With XeCℓ, XeBr, XeI, KrF and ArF, there is the possibility of Xe^* (or Kr^*, Ar^*, photoabsorption, as well as XeX self-absorption in XeCℓ and XeBr and XeI. In $Cℓ_2/XeCℓ^*$ mixtures, halogen absorption has to be overcome as well.

There is reason to hope that the efficiency of the rare gas halides will be quite large. To begin with, the quantum efficiency is very good. For example, in a laser in which the Xe metastable levels are pumped directly (as by e^- impact) the quantum efficiency (laser photon energy divided by Xe metastable energy) is approximately 42% for XeF. Similarly, in a system in which the Xe^+ ion is pumped, the quantum efficiency (laser photon energy divided by Xe ionization potential) is approximately 29% for XeF. For the other xenon halides the quantum efficiency will be even larger. The maximum efficiency which might be expected from pure electron-beam excitation can be estimated in the following way: For each 21.9 eV of energy deposited in Xe by an electron beam, one Xe^+ ion-electron pair is formed.[4] 12.1 eV of this energy is accounted for by the ionization potential of Xe. The remaining energy is split between excited states of Xe and kinetic energy of the secondary electrons. Theoretical calculations indicate that for each ion-electron pair formed, approximately one-half of an excited state of Xe is formed.[4] If we assume that each ion-electron pair and each excited state of Xe formed by the electron beam produce one laser photon, the overall efficiency is found to be approximately 24% for XeF. For the other xenon halides this number will be slightly better since the emission takes place at shorter wavelengths. For xenon/halogen mixtures diluted with argon, this number will be slightly smaller. For electron-beam stabilized discharge pumped lasers, the limiting efficiency is just the quantum efficiency (calculated above) based on the excitation of xenon metastable levels, namely 42%

The energy per pulse is limited by the consumption of F_2 by reactions 17 and 19. For XeF the maximum energy is 14 kilojoules per liter atmosphere of F_2. For a .1% mixture of F_2 in Xe, this corresponds to a pulse energy of 14 J/l-atm. The pulse repetition frequency will be limited by either the recombination rate of the halogen or the time required to purge the gas from the laser cell. In the first instance, if we require that a .1% mixture of halogen in Ar + Xe at a total density of $10^{20}/cm^3$ be 90% recombined before the next laser pulse, we find that the maximum pulse repetition frequency is $10^4/s$. This is based on a recombination coefficient of 10^{-32} cm^6/s which is appropriate for the halogens in argon at room temperature.[19] For a pulse energy of 10 J/l-atm, this corresponds to a specific power of 10^5 W/l-atm. A more severe limit on the pulse repetition frequency is imposed by the time required to purge the gas. This will be necessary if the temperature rise following the pulse is too great. For example, in a XeF laser producing 10 J/l-atm-pulse at an efficiency of 24%, the temperature rise will be approximately 100°C. If we assume a laser dimension of 30 cm in the flow direction and a flow velocity of 300 meter/s (corresponding to Mach 1 in argon at room temperature), the flow time is of the order of 1 ms. This will restrict the pulse repetition frequency to approximately $10^3/s$. For a laser operating at 1 atmosphere this corresponds to a power of 10^4 W/l. Clearly, these estimates are optimistic, but significant. On the basis of these simple considerations it would appear that the rare gas halide lasers are capable of satisfying ARPA's requirements.

REFERENCES

1. H. A. Koehler, L. J. Ferderber, D. L. Redhead and P. J. Ebert, Appl. Phys. Lett. 21, 198 (1972).

2. J. B. Gerardo and A. W. Johnson, IEEE J. Quantum Electroni, QE-9 (1973).

3. P. W. Hoff, J. C. Swingle and C. K. Rhodes, Opt. Commun. 8, 128 (1973).

4. D. C. Lorentz and R. E. Olsen, "Stanford Research Institute Semiannual Report for project PYU-2018 (December 27, 1972) (unpublished).

5. P. W. Hoff, private communication.

6. H. T. Powell, J. R. Murray and C. K. Rhodes, Appl. Phys. Lett. 25, 730 (1974).

7. D. L. Huestis, R. A. Gutcheck, R. M. Hill, M. V. McCusker, and D. C. Lorentz, "Studies of E-beam Pumped Molecular Lasers", Stanford Research Institute Report MP 75-18 (January 31, 1975) (unpublished).

8. D. L. King and D. W. Setser, "Quenching Studies of Ar ($^3P0$, $^3P2$) Metastable Atoms by Chlorine Atoms", presented at 4th Conference on Chemical and Molecular Lasers, St. Louis, MD (October 21-23, 1974).

9. M. F. Golde and B. A. Thrush, Chem. Phys. Lett. 29, 486 (1974).

10. J. J. Ewing and C. A. Brau, "Emission Spectrum of XeI* in Electron-Beam Excited Xe/I_2 Mixtures", to be published in Phys. Rev. A (July 1975).

11. J. E. Velazco and D. W. Setser, J. Chem. Phys. 62, 1990 (1975).

12. N. Bartlett and F.U. Sladky, "The Chemistry of Krypton, Xenon and Radon", in Comprehensive Inorganic Chemistry, Vol. I, A. F. Trotman-Dickinson, executive-ed. (Pergamon Press, Oxford, 1973).

13. R. C. Millikan and D. R. White, J. Chem. Phys. 39, 3209 (1963).

14. D. J. Seery and D. Britton, J. Phys. Chem. 68, 2263 (1964).

15. D. E. Rothe, Phys. Rev. 177, 93 (1969).

16. M. A. Biondi, "Charged Particle Recombination Processes", in DNA Reaction Rate Handbook, M. H. Bortner and T. Baurer, eds., Defense Nuclear Agency Report 1948H (March 1972).

17. R. M. Hill, R. A. Gutcheck, D. L. Huestis, D. Mukherjee and D. C. Lorentz, "Studies of E-beam Pumped Molecular Lasers", Stanford Research Institute Report MP 74-39 (July 31, 1974) (unpublished).

18. D. C. Lorentz, D. J. Eckstrom and D. Huestis, "Excimer Formation and Decay Processes in Rare Gases", Stanford Research Institute Report MP 73-2 (September 28, 1973) (unpublished).

19. V. H. Shi, J. P. Appleton and J. C. Keck, Thirteenth Symposium (International) on Combustion, p. 21, The Combustion Institute, 1971.

APPENDIX A

EMISSION SPECTRUM OF XeI* IN ELECTRON-BEAM-EXCITED Xe/I_2 MIXTURES

PHYSICAL REVIEW A VOLUME 12, NUMBER 1 JULY 1975

Emission spectrum of XeI* in electron-beam–excited Xe/I_2 mixtures*

J. J. Ewing and C. A. Brau
Avco Everett Research Laboratory, Inc., Everett, Massachusetts 02178
(Received 2 January 1975)

Emission spectra observed from electron-beam-excited atmospheric-pressure gas mixtures of Xe and I_2 are reported and analyzed in terms of an ionic alkali-halide-like excited state Xe^+I^-. A simple theory is given to analyze the observed spectra, and predictions of the uv spectra of other inert-gas monohalides are made. This class of molecules appears to offer interesting possibilities for production of new uv lasers.

INTRODUCTION

This paper describes the continuum emission spectrum of XeI* which is produced when mixtures of Ar/Xe/I_2 are irradiated with a high-intensity electron beam. A narrow band near 2535 Å is observed and assigned to the transition $(XeI)^*(^2\Sigma_{1/2}) \rightarrow XeI(^2\Sigma_{1/2})$. XeI is an unstable species which rapidly decays into Xe and I. Broader bands are observed at longer wavelengths, 3190 and 3610 Å, and are assigned to transitions which terminate on the $^2\Pi_{3/2}$ and $^2\Pi_{1/2}$ states of XeI. XeI* is a prototype of a set of inert-gas monohalides which should show similar emission continua in the ultraviolet region.[1]

A simple ionic-bonding model is used to predict that the primarily ionic molecule, Xe^+I^-, an excited state of XeI, is bound with respect to Xe and electronically excited $I(6s\,^1P)$. This "ionic" xenon halide, formed in our high-pressure experiments by rapid energy transfer and three-body processes, can radiate to the repulsive ground-state potentials of XeI. The ionic model can be used to estimate the binding energy of XeI* as well as the wavelengths of the emission bands which terminate on the repulsive lower-lying states. The diabatic Coulomb potential curve of Xe^+I^- crosses the Xe + I* potential curve at fairly large internuclear separations as shown in Fig. 1. This is not surprising since Xe* has an ionization energy comparable to the ionization energy of Cs, which forms ionic molecules with halogens. The large Coulomb binding energy leads to very large shifts in the molecular XeI spectra from the free-atom spectra. Such molecular emission bands could be ideal for an "excimer" or "molecular association" laser. XeI is not unique in this respect, and we make predictions of the approximate wavelengths for similar emission bands for other inert-gas halides.

EXPERIMENTAL DETAILS

Room-temperature mixtures of I_2 with Ar containing 8.5% Xe (total impurity limits ~5 ppm) and also I_2 with pure Xe (50-ppm impurities) were irradiated with a 0.4-MeV electron beam. The 1×15-cm^2 beam was produced by pulse charging a carbon cathode with a Marx generator (Ion Physics Corp.). The energy incident on the test gas is roughly 1 J/cm^2. The pulse time is 100 nsec. The primary electrons ionize and excite the Ar and Xe. This excitation eventually resides in the most bound excited electronic state which then radiates or is quenched. The kinetics of the latter is not yet known for Xe-I_2 mixtures, but three-body processes will be rapid at the pressures used and recombination into bound excited states occurs on a time scale of nanoseconds. Emission spectra were recorded on film (Kodak 103-O) using an $f/3.5$ Hilger quartz prism spectrograph with an entrance slit width of 100 μm; one to three shots gave sufficient film blackening. Time-resolved emission was observed with a 1P28 photomultiplier viewing the exit slit of a Spex 100-mm Micromate monochromator with a bandpass of typically 40 Å.

Figure 2 shows the emission spectrum of 25 lb/in.^{2} (absolute) of 8.5% Xe/Ar inert gas mixed with room temperature I_2 (density ~10^{16} cm^{-3}). These continuum bands do not appear when Ar/I_2 mixes are excited with the electron beam. Similarly, when mixtures of Xe and Ar or pure Xe without I_2 are irradiated, the continua are not observed.[2] Finally when pure Xe is mixed with I_2, the continuum bands are recovered. No evidence has been found on film or by photomultiplier of I_2 emission in the visible or uv. Since the continua require both I_2 and Xe but do not appear in Ar/I_2 mixtures, we conclude that they must arise from a xenon-iodine atom complex. Finally under the conditions of our experiment we do not anticipate that the I_2 will exist for very long during the electron-beam pulse. I_2 will be removed by the processes of energy transfer from Xe* and Xe_2^*, dissociative attachment by the slow electrons and photodissociation in the visible and most especially in the vacuum uv, where the Xe_2^* excimer band overlaps the I_2 $(X \rightarrow I)$ band.[3] Experimental study and detailed computer modeling of the kinetics of

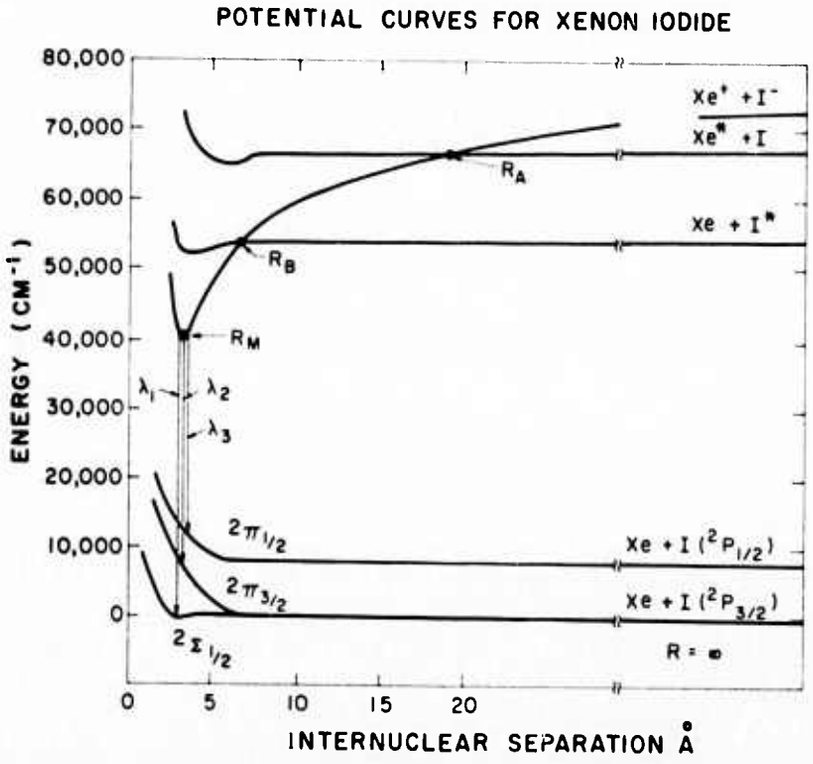

FIG. 1. Estimated potential curves for XeI.

these processes are currently under way.

The emission band at 2535 Å has a fairly sharp edge at ~2549 Å, and about 95% of the emission is found between about 2510 and 2549 Å. This band is noticeably asymmetric and shades off into the blue, indicating that the lower-state potential energy curve for this bound-to-free transition is not changing rapidly with internuclear separation. The 3190 and 3610-Å bands are broad and fairly symmetric, being ~1500 and 4120 cm^{-1} wide, respectively, probably terminating on strongly repulsive lower-state potentials.

IONIC MODEL FOR XeI*

The spectrum observed can be interpreted by the potential energy diagram shown in Fig. 1.

At infinite internuclear separation one has Xe + $I(^2P_{3/2})$ at zero energy, Xe + $I(^2P_{1/2})$ at 7819 cm^{-1}, Xe + $I(^4P)$ at 54633 cm^{-1} (labeled as Xe + I*), Xe($^3P_2$) + $I(^2P_{3/2})$ at 67078 cm^{-1} (labeled as Xe* + I), and $Xe^+ + I^-$ at 73128 cm^{-1}. $Xe^+ + I^-$ is lower in energy than $Xe^+ + e + I$ by an amount equal to the electron affinity of iodine.[4] For simplicity, only the lowest-lying excited states are shown. As R decreases the low-lying ^2P states are split into $^2\Sigma_{1/2}$, $^2\Pi_{3/2}$, and $^2\Pi_{1/2}$ states.[3] These molecular potentials should be repulsive at small R. The $^2\Sigma_{1/2}$ state lies lowest since the p orbital hole on the I atom points directly at the electron-rich Xe atom. The $^2\Pi$ states, however, put two p electrons in the immediate vicinity of Xe and hence should be considerably more repulsive than the $^2\Sigma_{1/2}$ state.

Similarly the ^2P Xe^+ and the ^1S I^- ions will produce $^2\Sigma_{1/2}$ and $^2\Pi_{1/2,3/2}$ states having the same order as the lower states for similar reasons. At

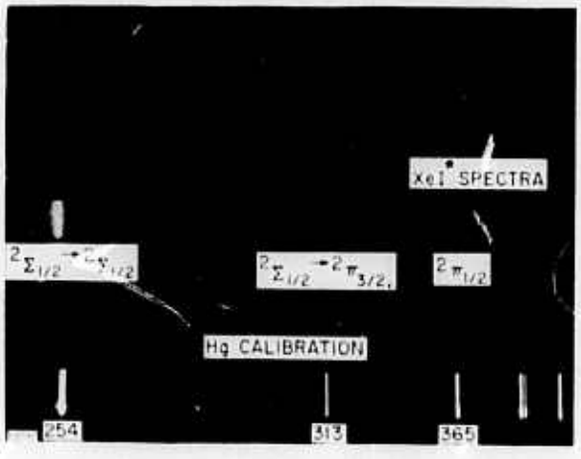

FIG. 2. Emission spectra of Ar/Xe/I_2 mixes. Top, 1 shot; middle, 3 shots; bottom, Hg calibration.

the minimum of the ionic curve, the $^2\Pi$ states of XeI* will probably be more than kT higher in energy than the $^2\Sigma$ ion state. At large R the energy of the ion pair is readily estimated by simple Coulomb attraction, while the Xe + I* and Xe* + I potential curves are flat. The zero-order ionic curve will cross, in a diabatic sense, all of the Xe* + I and I* + Xe curves at fairly large values of R, as in the more familiar case of alkali halide molecules.[5]

Table I lists the values of R at which these crossings occur for XeI and other inert gas monohalides. The crossing radii, in atomic units, are given by the expressions $R_A^{-1} = V_I(Xe^*) - EA(I)$ and $R_B^{-1} = V_I - EA - E_D$, where V_I is the ionization potential of the Xe excited state, EA the electron affinity of iodine, and E_D the energy gap between Xe* + I and Xe + I*, all energies being expressed in atomic units. These derive from the simple condition that the attractive Coulomb energy e^2/R be equal to the energy difference at infinite separation. Any deviation from flatness of the covalent potential or deviation from pure Coulombic attraction for the ion pair will alter this result of course. Deviations can be expected for crossings which would occur at small R. The closer crossing, R_B, may never occur for some of the inert-gas monohalides such as ArI. For XeI*, R_A and R_B are sufficiently large that the lowest excited state potential will be predominantly ionic in nature.

The ionic curve drops in energy to R_M, where short-range repulsion becomes important. We estimate R_M and E_M by noting that the nearly isoelectronic salt CsI has comparable ionic binding, and that Cs^+ and Xe^+ ions should have about the same size. R_M for gaseous CsI is 3.32 A,[6] and the binding energy relative to ions is 97.4 kcal/mole.[7] Subtracting the CsI binding energy from $E(Xe^+ + I^-)$ gives E_M of 39135 cm^{-1}. E_M would be 39135 cm^{-1}. Using this E_M one predicts emission to occur at 2555 A if the lower $^2\Sigma_{1/2}$ state has zero energy at R_M. Since the 2535-A band is very narrow and has a sharp long-wavelength edge, the presumption that the lower $^2\Sigma$ state is flat at R_M is probably good. The predicted emission wavelength is within 1% of observed; so for estimating the spectra of other inert gas monohalides we will use the binding energy of the nearest alkali halide. The observed $^2\Sigma \rightarrow {}^2\Sigma$ band position and shape implies $E_M(XeI^*)$ is actually 39 450 cm^{-1}.

One can use the observed positions and spectral widths of the XeI* bands to estimate the lower-state energies and potential gradients at R_M. In the upper state roughly 95% of the molecules will be in vibrational states, $v = 0, \ldots, 4$, assuming a vibrational temperature of 300 K. Using the molecular constants of CsI, we estimate the spread in R accessible to the XeI* molecules from the rms value of $(R - R_M)/R_M$ for a harmonic oscillator.

TABLE I. Estimated features of inert-gas monohalides.

Molecule	R_A (A)	R_B (A)	R_M (A)	E_M (cm^{-1})	λ_1 (nm)	λ_2 (nm)	λ_3 (nm)
XeI	19.2	6.3	3.3	39 135	256	302	342
XeBr	32.0	15.9	3.1	34 272	292	354	407
XeCl	71.9	a	2.9	30 860	324	402	417
XeF	39.6	a	2.35	25 895	386	503	512
KrI[b]	14.1	3.5	3.2	54 000	185	208	247
KrBr	19.9	5.2	2.9	49 353	203	231	252
KrCl	30.5	9.8	2.8	45 592	219	253	258
KrF	22.7	a	2.27	39 229	256	301	305
ArBr[c,b]	17.0	3.2	2.8	62 152	161	178	190
ArCl[c,d]	24.1	4.5	2.7	58 042	172	192	195
ArF[c]	18.9	a	2.17	37 484	267	318	322
NeF[c,b,e]	9.6	2.6	1.93	93 266	107	115	115

[a] These species have halogen excited-state levels only above the inert-gas excitation levels. Hence no R_B crossing occurs.

[b] These species will not be as "ionic" as those with large R_B.

[c] These spectra could be complicated due to multiple excited states because of the smaller spin orbit splitting in Ar^+ and Ne^+.

[d] The ArCl bands appear at 170 nm (λ_1) and 175 nm (λ_2, λ_3) in low-pressure discharge flow experiments, Ref. 9; λ_1 apparently is predicted within 1% while λ_2, λ_3 are within 10%.

[e] For ArI, NeI, NeBr, NeCl, and the helium halides the inert-gas ionization potential is so large that the Coulomb curve does not make up sufficient energy to approach the low-lying halogen excited states. These compounds should only have small well depths and the molecular continua should be near the free atom lines. Possibly ionic states of the opposite polarity, viz. $Ne^- + I^+$, could enter into the binding.

$[2B\omega^{-1}(v+\frac{1}{2})]^{1/2}$, apparently an adequate estimate for the alkali halides.[8] We calculate a total R width of 0.3 Å for $v=4$. From the plates, we estimate the 95% widths to be 650 cm^{-1}, 1500 cm^{-1}, and 4120 cm^{-1}. The width of the bands in excess of $2kT$ is attributable to a slope in the lower-state potential curve. For $^2\Sigma_{1/2}$ the slope is about 670 cm^{-1} $Å^{-1}$, again indicating that this state is not in the region of strong repulsion at R_M. The $^2\Pi_{3/2}$ slope is estimated to be 5000 cm^{-1} $Å^{-1}$, $^2\Pi_{1/2}$ is 13 700 cm^{-1} $Å^{-1}$. We do not understand why the $^2\Pi_{1/2}$ band is broader.

The center of the $^2\Pi$ bands locates the energies of these repulsive states at R_M. $^2\Pi_{3/2}$ is at about 8100 cm^{-1}, while $^2\Pi_{1/2}$ is ~4150 cm^{-1} above its separated-atom limit of $^2P_{1/2}$.

These pieces of information then can be used to make crude estimates of the emission spectra of the other inert-gas monohalides as given in Table I. The rules for obtaining Table I are: E_M is determined by subtracting the bond energy of the nearest alkali halide from the infinite-R ion pair energy (CsBr is used for XeBr*, etc.); R_A and R_B are obtained by assuming the covalent potentials are flat for all R; the $^2\Sigma \rightarrow {}^2\Sigma$ band position is estimated by assuming the $^2\Sigma_{1/2}$ ground state has zero energy at R_M; the $^2\Pi$ states energies at R_M are estimated to be 6000 cm^{-1} (the average of our $^2\Pi_{3/2}$ and $^2\Pi_{1/2}$ XeI repulsions) above their respective infinite-separation values. We feel these estimates will predict the emission wavelengths to within 10%, and future measurements should give better estimates of the potentials of other inert-gas halides.

Note added. Since the submission of this paper a communication by Velazco and Setser[10] has appeared substantially confirming the predictions for the $\Sigma - \Sigma$ bands of XeCl, XeBr, and XeF. Peak wavelengths appear at: XeI, 252 nm; XeBr, 278 nm; XeCl, 304 nm; and XeF, 346 nm. The spectra they observe are broader since their work is done at low pressures and they observe emission from species which do not have time to vibrationally relax before emitting uv photons. The peak wavelengths are in agreement with recent data on these species obtained in our high-pressure experiments. Also a paper by Golde and Thrush[11] on ArCl emission has appeared making many of the same arguments about the ionic binding in this molecule. As pointed out in the table, the wavelength for ArCl emission is in good agreement with our prediction for the $\Sigma - \Sigma$ transition.

---

*This work was supported by Advanced Research Projects Agency, Department of Defense, and monitored by Office of Naval Research under Contract No. N00014-75-C-0063.

[1]D. L. King and D. W. Setser, in Fourth Conference on Chemical and Molecular Lasers, St. Louis, 1974, Paper WA1 (unpublished).

[2]We do see the XeO "auroral line" continua in the green, and an unidentified band near 3290 Å when "pure" Ar/Xe or Xe is excited with the electron beam.

[3]G. Herzberg, *Spectra of Diatomic Molecules* (Van Nostrand, Princeton, N.J., 1963); R. S. Mulliken, J. Chem. Phys. 55, 288 (1971); J. A. Myer and J. A. R. Samson, *ibid.* 52, 716 (1970).

[4]C. E. Moore, *Atomic Energy Levels*, Natl. Bur. Stds. Circ. 467 (U.S. GPO, Washington, D.C., 1962); R. S. Berry and C. W. Reimann, J. Chem. Phys. 38, 1540 (1963).

[5]J. L. Magee, J. Chem. Phys. 8, 6817 (1940); R. S. Mulliken, Phys. Rev. 50, 1017 (1963); 50, 1028 (1963).

[6]C. H. Townes and A. L. Schawlow, *Microwave Spectroscopy* (McGraw-Hill, New York, 1955).

[7]Y. P. Varshni and R. C. Shukla, J. Mol. Spectrosc. 16, 63 (1965).

[8]S. A. Rice and W. Klemperer, J. Chem. Phys. 27, 573 (1957).

[9]D. H. Stedman and D. W. Setser, Prog. React. Kinet. 6, 193 (1971).

[10]J. E. Velazco and D. W. Setser, J. Chem. Phys. 62, 1990 (1975).

[11]M. G. Golde and B. A. Thrush, Chem. Phys. Lett. 29, 486 (1974).